ELSEVIER

Contents lists available at ScienceDirect

Journal of Cleaner Production

journal homepage: www.elsevier.com/locate/jclepro





Particle deposition and clogging as an Obstacle and Opportunity for sustainable energy

Mehryar Amir Hosseini^a, Pejman Tahmasebi^{a,*}

a Colorado School of Mines, Golden, CO, 80401, USA

ARTICLE INFO

Handling Editor: Panos Seferlis

Keywords:
Fine particle
Clogging
Energy optimization
Sustainable resources
Computational fluid dynamics
Discrete element method

ABSTRACT

Fine particle motions have significant implications in porous media, manifesting in various natural phenomena and industrial applications. The movement of particles can lead to channel blockage, resulting in clogging. Depending on the context, clogging can be either advantageous or detrimental. At the scale of fine particles, physiochemical interactions play a crucial role in the clogging process. To examine the influence of these interactions, we have coupled the Derjaguin-Landau-Verwey-Overbeek (DLVO) theory into the Computational Fluid Dynamic-Discrete Element (CFD-DEM) approach. Aside from the physical properties of the fracture systems and the characteristics of fine particles, the injection rate also plays a pivotal role in clogging occurrence. Consequently, we investigated 10 different injection rates and modeled 20 simulation setups with identical particle insertion rates to concurrently analyze the effects of the DLVO theory and injection rate. Our study focused on examining the impact of these parameters on particle behavior in various regions of the domain, including particle-particle force, fluid-particle force, transitional velocity, rotational velocity, fluid velocity, and fluid-particle momentum exchange. Our findings reveal that the DLVO force significantly influences fluid and particle characteristics within the throat blockage. Our results indicated that DLVO consideration increased the particle concentrations by more than 40% before the throat. Moreover, our results demonstrate a transition between different injection rates, where a slight change in injection rate (i.e., $0.06 \, \mu m/s$) can change the system's behavior. We identified a critical fluid injection rate, whereby injecting fluid into the system at a rate surpassing the critical velocity can prevent clogging, while lower rates result in clogging occurrence.

1. Introduction

Granular materials, composed of discrete, macroscopic particles, exhibit fascinating and complex behaviors that have intrigued scientists and engineers alike. From powders and grains to sands and soils, granular substances are ubiquitous in nature and industry. Understanding their dynamics is crucial for various applications, as these materials can behave like solids, liquids, or gases depending on the context. The properties and applications of such materials across different fields and environments are reviewed elsewhere (Tahmasebi, 2023). In the realm of granular flows, a noteworthy phenomenon is clogging—a process where the smooth movement of particles through a confined space is disrupted, leading to the formation of blockages. Clogging can manifest in diverse scenarios, from industrial hoppers handling powders, filtration systems processing grains, to energy production. The mechanisms behind clogging involve intricate interactions between particle properties, environmental conditions, and the confinement geometry.

Investigating clogging in granular materials is not only a scientific pursuit but also holds practical significance for optimizing processes and systems that involve the controlled flow of these fascinating materials.

The movement of fine particles has been extensively studied in various fields, including pore-clogging (Lin et al., 2021; Todisco et al., 2023), microfluidic systems (Dincau et al., 2022; Gaol et al., 2021), energy extraction (Xia et al., 2023), groundwater (Hou et al., 2023; Ye et al., 2022), sediments fracturing (Daigle et al., 2020; Shin and Santamarina, 2010), geothermal systems (Cui et al., 2022; Liu et al., 2019), hydrate-bearing sediments gas production (Fang et al., 2022; Liang et al., 2020), biological systems (Pang et al., 2015), filtration (Markiewicz et al., 2022), fractured systems (Kang et al., 2022; Li et al., 2022), etc. The impact of clogging can vary depending on the specific context. In some cases, clogging is undesirable as it reduces the efficiency and lifespan of the system, particularly in fabrication applications and also when one aims to produce fluid from a subsurface system (i.e., energy production) since particles can accumulate and form deposits, leading to reduced permeability and fluid flow (Xia et al., 2023). However,

E-mail address: tahmasebi@mines.edu (P. Tahmasebi).

^{*} Corresponding author.

Nomenclature Parameters		$ ho_f$	v_f Fluid velocity (m/s)	
		-		
$egin{array}{l} m{m}_i & m{v}_i & m{r}_i^{p-p} & m{f}_i^{f-p} & m{f}_i^{f-p} & m{f}_i^{f} & m{r}_i & m{g}_i^{f} & m{r}_i & m{g}_i^{f} & m{r}_i & m{g}_i^{f} $	Mass of particle i (kg) Transitional velocity of particle i (m/s) Particle-particle force applied on particle i (N) Fluid-particle force applied on particle i (N) Gravitational force applied on particle i (N) Rotational inertia of particle i ($kg.m^2$) Rotational velocity of particle i (rad/s) Torque acting on particle i because of its collision with particle j ($N.m$) Torque acting on particle i caused by fluid ($N.m$) Non-contact force between particle i and j (N) Contact force between particle i and j (N) Tangential force between particle i and j (N) The van der Waal force (N) Normal stiffness (N/m) Particles overlap (m) unit vector of normal force ($-$) Normal damping (kg/s) Relative velocity of particle i and j (m/s) Tangential spring's stiffness (N/m) Tangential damping (kg/s) Friction coefficients ($-$)	$egin{array}{l} p & & & & & & & & & & & & & & & & & & $	Pressure (<i>Pa</i>) Stress tensor (N / <i>m</i> ²) Gravity force (<i>N</i>) Momentum exchange between fluid and particle (<i>kg.m</i> / <i>s</i> Pressure gradient (<i>N</i>) Drag force (<i>N</i>) Viscous force (<i>N</i>) Volume of particle (<i>m</i> ³) Pressure gradient (<i>Pa</i> / <i>m</i>) Drag coefficient (–) Particle velocity (<i>m</i> / <i>s</i>) Torque coefficient (–) Relative rotational velocity (<i>rad</i> / <i>s</i>) Reynolds Number of relative angular velocity (–) Before throat length (<i>m</i>) After throat length (<i>m</i>) Channel width (<i>m</i>) Channel width (<i>m</i>) Throat width (<i>m</i>) Throat length (<i>m</i>) dimensionless average fluid velocity difference (–) the normalized momentum exchange (–)	
$\frac{\mu}{\overrightarrow{u}_t}$	Unit vector of tangential force (–)	DLVO	Direct Numerical Simulation	
	Cut off radius (<i>m</i>)	E-E	Eulerian-Eulerian	
$r_{cutoff} \ A_i$	Hamaker constant for particle $j(J)$	E-L	Eulerian-Lagrangian	
r_i	Radius of particle $i(m)$	CFD	Computational Fluid Dynamic	
r_j	Radius of particle $j(m)$	DEM	Discrete Element Method	
H_{ij} $lpha_f$	Distance between particle i and j (m) Fluid fraction ($-$)	SPH	Smoothed-Particle Hydrodynamics	

clogging can also be a beneficial outcome when used as a reinforcement technique or in energy storage (e.g., leakage remediation) and geothermal applications (Bagheri et al., 2019; Dalla Vecchia et al., 2020). As such, understanding the dynamics of clogging and its influence is crucial for optimizing these systems. By investigating the behavior of fine particles and the mechanisms leading to clogging, one can develop strategies to prevent or control clogging, thereby improving the overall performance and reliability of the applications.

There are three well-known mechanisms that can lead to clogging: aggregation of particles, sieving, and bridging. When particles continuously displace and block a microchannel, it is categorized as clogging by aggregation. In this mechanism, particles that are in close proximity attract each other, resulting in the formation of particle clusters. These clusters then jam the pore-throat, leading to clogging (Giglia and Straeffer, 2012; Zhang et al., 2015). Sieving, on the other hand, occurs when the particle size is significantly larger than the width of the microchannel (Berthet et al., 2013; Duru and Hallez, 2015). In this case, the particles themselves act as a physical barrier, preventing the passage of fluid and causing clogging. Bridging is another clogging mechanism that occurs when the particle size is smaller than the dimensions of the microchannel. Unlike aggregation, bridging involves the formation of a clog with a smaller number of particles (Divoux et al., 2015; Zuriguel et al., 2014). It is important to note that in aggregation and bridging scenarios, the flow characteristics can influence the clogging process. However, in sieving, the flow properties do not play a significant role in clogging. Understanding these mechanisms and their associated flow dynamics is crucial for effectively managing and mitigating clogging in

microchannel and tight fracture systems.

During the clogging process, there is competition between different forces, namely the fluid-particle force, particle-particle force, and particle-wall force. If the fluid-particle force is strong enough to overcome the other forces, clogging may be avoided. However, if the fluid flow is unable to break the particle-particle and/or particle-wall bonding, the clogging or deposition process begins. It is important to note that in sieving, where the throat width is smaller than the particle size, clogging is inevitable regardless of the fluid force. The clogging process involves a combination of deposition, resuspension, and clustering. Deposition occurs when the fluid-particle force moves a particle close to the wall, leading to particle-wall bonding. If the particle-wall bonding is not strong enough to withstand the fluid force, resuspension occurs. Among these mechanisms, clustering has been identified as the primary cause of clogging. Previous investigations have shown that the deposition of a single particle can give rise to multiple clusters, ultimately leading to clogging (Henry et al., 2012).

The understanding of the clogging process in micro-scale systems is still limited due to the complex interactions between fluid particles, particle-particle interactions, and particle-wall interactions. Experimental studies have explored various factors influencing clogging, such as the particle-to-pore throat size ratio (Marin et al., 2018), particle concentration (Wyss et al., 2006), path tortuosity (Bacchin et al., 2014), and initial retardation (Valdes and Carlos Santamarina, 2007). However, conducting experimental investigations to capture the behavior of microparticles, fluid, and their interactions can be challenging and costly. Numerical simulations provide an efficient alternative for

studying clogging in microparticles. In these simulations, it is essential to consider the physicochemical forces at play. The Derjaguin-Landau-Verwey-Overbeek (DLVO) theory, which includes attractive van der Waals forces and repulsive Electrostatic Double Layer forces, can be implemented to capture these forces (Dressaire and Sauret, 2016). Previous studies have highlighted the influence of van der Waals forces on clogging. Contrary to the importance of such force (i.e., van der Waals) in clogging, the lack of numerical study on the influence of injection rate in such fluid-particle systems, when considering DLVO theory, can be seen in the literature. A summary of numerical studies is given in Table 1 wherein the pros and cons are also highlighted.

To fill the existing research gap, therefore, this paper aims to develop a numerical approach to investigate the impact of the DLVO theory and flow rate on clogging, aiming to identify the critical injection rate at which blockage can be expected in the domain. First, we will discuss available numerical methods and select the one that offers the most advantages. Subsequently, we will conduct a comprehensive study on the influence of the injection rate on inter-particle and fluid-particle interactions to determine the minimum flow rate that leads to clogging.

When developing numerical schemes to study clogging, it is crucial to consider the interactions between particles, walls, and fluid, as they significantly influence the clogging process. Several well-known methods can be used to capture these interactions: Direct Numerical

 Table 1

 Summary of numerical investigations on the clogging process.

Reference	Detail
Agbangla et al. (2014)	A Force Coupling Method (FCM) was applied to study clogging with the DLVO considerations. The flow rate was kept constant, and the formation of clogging was discussed. This work indicated that the FCM needs to be corrected for more than 20% particle concentrations.
Mondal et al. (2016)	A resolved CFD-DEM technique has been used to model the particle suspension flow. The jamming process with regard to particle concentration, outlet size, inlet size, and three flow rates are studied. The diameter of particles was 2 mm, and the DLVO is not considered.
Zhou et al. (2018)	LBM-DEM-IMB simulations were conducted on particle clogging under different particle diameters, concentrations, and particle's flow rates. The DLVO theory effect is not considered here.
Sun et al. (2019)	CFD-DEM approach was applied to simulate the clogging process. Here, the DLVO theory was not considered in the simulations, and the diameter of particles was from 0.45 mm to 2 mm.
Xu et al. (2020)	CFD-DEM technique has been applied to study the influence of jamming in the pore geometry with a lognormal particle distribution. Particle diameter size varies from 0.56 mm to 0.68 mm. The flow rate is kept constant, and the DLVO's impact was not studied.
Song et al. (2021)	Simulations are conducted using CFD-DEM to study the clogging in the gravitational system while considering the ellipsoidal and spherical particles. Particle diameter was selected to be 2.39–2.80 mm.
Lin et al. (2022)	CFD-DEM approach has been used to study granular lost circulation materials. Here, sealing properties (e.g., sealing time) have been investigated for particle diameters between 0.1 mm and 1.0 mm. The impact of the fluid-particle force and particle properties (e.g., size) were studied. The DLVO consideration has been neglected in this study.
Di Vaira et al. (2023)	A direct numerical simulation approach has been applied to study hydrodynamic clogging in planar channels while considering DLVO theory.
Saparbayeva and Balakin (2023)	CFD-DEM has been applied in the simulations, and the Johnson-Kendall-Roberts (JKR) model is added to formulations to consider the cohesion between particles. The DLVO consideration has not been studied in this work. Moreover, the particle size was selected as 400 µm.
Yin et al. (2024)	LBM-DEM-IMB simulation conducted on the clogging process for different pore geometry. The influence of DLVO theory is neglected in this study, and the diameter of particles was set to be 1 mm.

Simulation (DNS) (Baker et al., 2020), Eulerian-Eulerian (E-E) approach (Baker et al., 2020; Lee and Lim, 2017), and Eulerian-Lagrangian (E-L) coupling (Amir Hosseini et al., 2023; Knight et al., 2020). DNS involves solving Newton's equations for individual particles and the Navier-Stokes equations for the fluid phase. However, DNS requires high computational power and is generally suitable for systems with a small number of particles. The E-E approach treats both the solid and fluid phases as a continuum, which is not realistic for modeling individual particles since their behavior can differ significantly in response to fluid motion. While the E-E approach can be applied to large-scale problems, it does not accurately capture microscale forces such as DLVO interactions since particles are not treated separately. In contrast, the E-L approach considers each particle as a distinct object and employs a Lagrangian framework for particle analysis, while the fluid phase is modeled as a continuum using an Eulerian approach. This method allows for the simulation of fluid flow using local averaging techniques. Various approaches are commonly employed to simulate fluid-particle interactions within the E-L framework, including LBM-DEM (Lattice Boltzmann Method-Discrete Element Method) (Han and Cundall, 2013), CFD-DEM (Computational Fluid Dynamics-Discrete Element Method) (Amir Hosseini et al., 2023; Li and Zhao, 2018; Tahmasebi and Kamrava, 2019; Zhang and Tahmasebi, 2018, 2019), LES-DEM (Large-Eddy Simulation-Discrete Element Method) (Elghannay and Tafti, 2018; Zhou 2017), and SPH-DEM (Smoothed-Particle Hydrodynamics-Discrete Element Method) (El Shamy and Sizkow, 2021; Xu and Dong, 2021). These approaches offer different advantages and can be applied based on the specific requirements of the study. A comprehensive review on these methods in granular systems can be found elsewhere (Tahmasebi, 2023).

Among the mentioned methods, the CFD-DEM coupling approach is widely used in various fields and scales. It combines the strengths of CFD and DEM by assigning the fluid and solid calculations to CFD and DEM, respectively. The accuracy of CFD-DEM coupling has been demonstrated in numerous studies found in the literature. In CFD-DEM, Newton's second law is solved to determine the trajectory of each particle, making the DEM calculations computationally demanding. However, with advancements in computer power, this approach has become more feasible and commonly used. This approach is particularly suitable for considering different types of inter-particle interactions, including DLVO forces, making it well-suited for studying clogging processes and the influence of the DVLO theory. To this end, therefore, we extended the capacity of the existing CFD-DEM coupling approach to include DLVO in the clogging process modeling. By developing and implementing the CFD-DEM approach, we aim to better understand the micro-scale clogging phenomena.

The rest of this paper is organized as follows. Section 2 provides a description of the governing equations for CFD, DEM, and their coupling. In Section 3, we present the details of the domain dimensions, particle and fluid properties, and the range of injection rates considered in our study. Section 4 presents the results obtained from our investigation, which are presented and discussed in detail. Finally, in Section 5, we summarize the key findings of our study and provide a conclusion.

2. Numerical method

In this section, we will introduce the fundamental numerical approach adopted in our study. We begin by discussing the governing equations used in the DEM, taking into account the van der Waals attraction force based on the DLVO theory. Then, we present the numerical method employed for CFD simulations. Following that, we describe the equations governing the fluid-particle interactions and present various approaches for solving these interactions.

2.1. DEM: governing equations

The Discrete Element Method (DEM) (Cundall and Strack, 1979)

simulates the motion of individual particles and the forces acting between them. In this method, each particle in the computational domain can undergo translational and/or rotational motion. DEM calculates the momentum and energy exchange between particles during collisions. Additionally, non-contact forces, which do not involve direct particle-particle contact, are also considered. In this study, we incorporated both contact and non-contact forces in the DEM. After calculating the inter-particle forces at each time step, the DEM determines the movement of each particle by applying Newton's laws of motion to calculate their trajectories. In this section, we will describe the equations of motion for particle-particle interactions and particle-wall interactions. These equations govern the behavior of particles and their response to external forces.

Newton's equations of motion for particle i is described by (Cundall and Strack, 1979):

$$m_i \frac{dv_i}{dt} = f_i^{p-p} + f_i^{f-p} + f_i^g \tag{1}$$

$$I_i \frac{d\omega_i}{dt} = \sum_j T_{ij} + T^{f-p} \tag{2}$$

where Eq. (1) shows the transitional motion of particle i with a mass of m_i and transitional velocity (v_i) . Moreover, the particle-particle and/or particle wall interactions on particle i are defined as f_i^{p-p} . The effect of the existence of the fluid and gravity are also considered in fluid-particle force (f_i^{f-p}) and gravitational force (f_i^g) , respectively. In Eq. (2), the rotational motion of particle i when it has a collision with particle j is presented, where, I_i and ω_i are rotational inertia and velocity, respectively. T_{ij} is the torque acting on particle i because of its collision with walls and/or particle j, and T^{f-p} is the torque which is caused by the fluid. Fig. 1 illustrates the forces and torques acting on particle i, providing a visual representation of the various interactions involved.

The linear spring and dashpot system is considered for inter-particle forces (Cundall and Strack, 1979). In this work, therefore, the

particle-particle forces (f_i^{p-p}) are:

$$f_i^{p-p} = f_{ii}^{nc} + f_{ii}^c = f_{ii}^n + f_{ii}^t + f_{ii}^{vdW},$$
(3)

where f_{ij}^{nc} is the non-contact force, f_{ij}^{c} is the contact force, f_{ij}^{n} is the normal contact force, f_{ij}^{t} is the tangential force, and f_{i}^{vdW} is the van der Waal attraction force for considering the DLVO theory.

To calculate the f_{ij}^n , the linear spring-dashpot contact model has been implemented in the DEM framework:

$$f_{ij}^{n} = -\left(k_{n}\delta\overrightarrow{u}_{n} + \alpha_{n}\left(\overrightarrow{v}_{ij}.\overrightarrow{u}_{n}\right)\overrightarrow{u}_{n}\right),\tag{4}$$

where k_n is the normal stiffness, δ is the particles overlap, \overrightarrow{u}_n is the unit vector of normal force, α_n is normal damping, and \overrightarrow{v}_{ij} is the relative velocity of in-contact particles i and j. Moreover, the tangential force is expressed by:

$$f_{ij}^{t} = min\left\{ \left(-k_{t}\delta + \alpha_{t} \left(\overrightarrow{v}_{ij} \times \overrightarrow{u}_{n} \right) \times \overrightarrow{u}_{n} \right); \mu \middle| \overrightarrow{f}_{ij}^{n} \middle| \overrightarrow{u}_{t} \right\},$$
 (5)

where k_t is tangential spring's stiffness, α_t and μ are tangential damping and friction coefficients, respectively. Also, \overrightarrow{u}_t is the unit vector of tangential force. The van der Waals force (f_i^{vdW}) is exerted on particles when they are in contact or sufficiently close to each other $(\leq r_{cutoff})$, which can be expressed as (Hamaker, 1937):

$$f_i^{vdW} = \sum_{j=1}^{N} -\frac{A_j r_i r_j}{6H_{ij}^2 (r_i + r_j)^2} \hat{e}_{ij},$$
 (6)

where N is the number of particles for which the distance between them and particle i is less than r_{cutoff} . Also, A_j is the Hamaker constant for particle j, r_i and r_j are particle i and j radius, respectively, H_{ij} is the distance between particle i and j, and \hat{e}_{ij} is the normal unit vector.

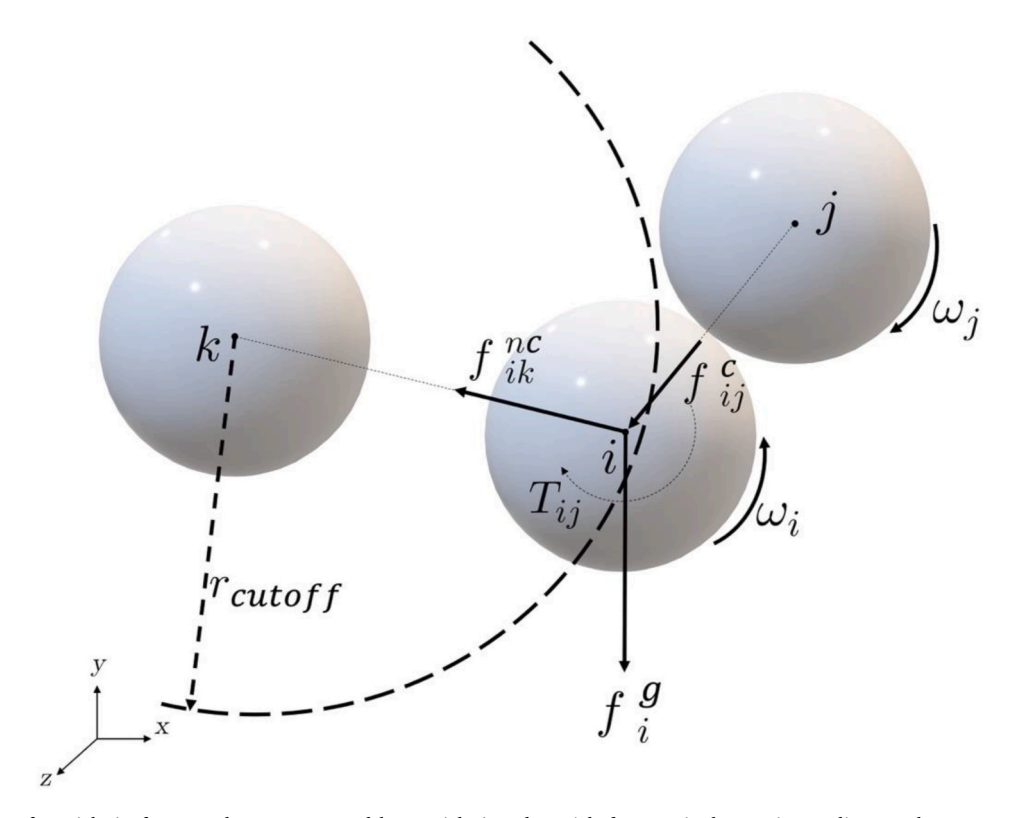


Fig. 1. Demonstration of particle *i*'s forces and torques exerted by particle *j*, and particle *k*. r_{cutoff} is the maximum distance that non-contact forces can affect surrounding particles.

2.2. CFD: governing equations

As discussed, the fluid phase is solved using the governing equations of Computational Fluid Dynamics (CFD). These equations are responsible for calculating the pressure, viscous force, and drag force within the domain to observe the influence of the fluid phase on the solid phase. To accomplish this, the domain is discretized into a mesh, and flow characteristics are calculated within each cell. The locally averaged Navier-Stokes equations are employed to describe the motion of the fluid phase. The equations governing the fluid phase within the domain are as follows:

$$\frac{\partial \alpha_f \rho_f}{\partial t} + \nabla \cdot (\alpha_f \rho_f) = 0, \tag{7}$$

$$\frac{\partial \left(\alpha_{f}\rho_{f}v_{f}\right)}{\partial t} + \nabla \cdot \left(\alpha_{f}\rho_{f}v_{f}\right) = -\alpha_{f}\nabla p + \nabla \cdot \left(\alpha_{f}\tau\right) - M^{f-p}\left(\alpha_{f}\tau\right) + f_{g},\tag{8}$$

where α_f is the fluid fraction in the cell, ρ_f is the fluid density, v_f is the fluid velocity, p is pressure, τ is the stress tensor, f_g is the gravity force, and M^{f-p} is the implicit momentum exchange between fluid and particle.

2.3. CFD-DEM coupling: governing equations

To calculate the influence of the particles on the fluid, the fluid-particle force exchange should be considered. In this work, therefore, the pressure gradient (f_p) , the drag (f_d) , and the viscous (f_v) forces are considered. So, fluid-particle interaction (f_i^{f-p}) can be defined as (Kloss et al., 2012)

$$f_i^{f-p} = f_p + f_d + f_v, (9)$$

where:

$$f_p = -V_p \nabla P, \tag{10}$$

$$f_d = -C_{drag} |v_f - v_p|, \tag{11}$$

$$f_{\nu} = -V_{p}(\nabla . \tau), \tag{12}$$

where V_p is the volume of the particle, ∇P is the fluid pressure gradient, C_{drag} is the drag coefficient, and v_p is particle velocity. In this work, we implemented the Huilin and Gidaspow drag coefficient (Huilin and Gidaspow, 2003) to calculate C_{drag} , which is the combination of the previously introduced correlations (i.e., Wen's (Wen, 1966) and Ergun's (Ergun, 1952)).

Furthermore, the fluid-particle torque (T^{f-p}) can be expressed as follows:

$$T^{f-p} = \frac{1}{2} \rho_f C_T |\omega_{rel}| \omega_{rel} (r_i)^5, \tag{13}$$

where C_T is the torque coefficient and ω_{rel} is the relative rotational velocity of fluid and particle. C_T can be described by:

$$C_T = \frac{128.64}{Re_{\omega_{rel}}} \left(1 + 0.1005 \sqrt{Re_{\omega_{rel}}} \right), \tag{14}$$

where Reynolds Number of relative angular velocity ($Re_{\omega_{rel}}$) is given by:

$$Re_{\omega_{rel}} = \frac{4\rho_f r_i |\omega_{rel}|}{v_f}.$$
 (15)

2.4. Coupling Algorithm

In this paper, we implemented the CFD-DEM coupling as follows.

- (1) The CFD, DEM, and coupling methods are initialized based on the initial boundary conditions. In the case of CFD, the initial condition involves specifying the positions of the fluid elements within the domain. On the other hand, for DEM, the positions of the particles are determined based on their initial coordinates. These initial conditions set the starting configurations for the fluid and particle phases in the simulation.
- (2) Each fluid cell's porosity (volume fraction) (i.e., the CFD mesh) is calculated, and the cell dedicated to each particle is recognized.
- (3) Forces caused by fluids (f_i^{f-p}) acting on particles are calculated. Fluid-particle interaction forces are also applied to particles on each fluid cell based on averaging in fluid cells.
- (4) Particle-particle (f_i^{p-p}) and fluid force on particles are solved for each DEM time step to reach the CFD time step.
- (5) After the DEM calculations, new positions and velocities of particles are transferred to the next time step of the CFD solver. The mass and momentum equations use each CFD cell's calculated porosity and fluid-particle interaction force. This step's results are the fluid phase's pressure and velocity fields.
- (6) The previous steps are repeated until the end of the simulation time.

3. Simulation setup

In this section, we will present the simulation setups that were employed to study the clogging process using the implemented method. To achieve the objectives of this study, it was necessary to design a geometry that closely mimics the structure of a pore and pore-throat within the system. Thus, we adopted the geometry depicted in Fig. 2. This figure illustrates that the domain can be divided into three distinct regions: (i) the region before the throat, (ii) the throat region itself, and (iii) the region after the throat. The dimensions of the domain can be found in Table 2. Additionally, the parameters for the fluid and particles used in the simulations can be found in Table 3 and Table 4, respectively. We must mention that the ratio of particles' diameter to throat size (i.e., 0.6) was selected based on the previous studies (Cao et al., 2019). As shown in Tables 3 and 4, the density of fluid and particles are selected equally to eliminate the influence of gravitational settlement on our analysis based on the previous works' recommendations (Baiyu et al., 2021; Tomac and Gutierrez, 2014).

To examine the impact of the injection rate on the clogging process, we considered 10 different injection rates. A summary of the simulations conducted can be found in Table 5. In Table 5, Case #4's injection rate is selected based on the previous studies (Prempeh et al., 2020), then we gradually changed the injection rate by $\pm 0.06~\mu\text{m/}_{\text{S}}$ to capture the influence of the injection rate systematically. Furthermore, in order to thoroughly explore the influence of the DLVO force on clogging, we conducted additional simulations without considering the DLVO force for each injection rate.

4. Results and discussion

This section presents the results obtained from the developed method regarding the clogging process. The focus is on analyzing the impact of the DLVO (van der Waals) force and injection rate. The injection rates for the studied cases are shown in Table 5. As mentioned earlier, our objectives are to probe the influence of the DLVO force on the clogging process and determine the critical injection rate.

Fig. 3 illustrates the time evolution of particle movement for one of the simulation cases (Case #5), comparing the scenarios with and without the consideration of the DLVO force. The results show that clogging occurs when the DLVO force is taken into account; see Fig. 3 (a), (c), and (e). In contrast, no clogging is observed in the simulations where the DLVO force is not considered. Moreover, in the cases involving DLVO force, particle accumulations can be observed not only

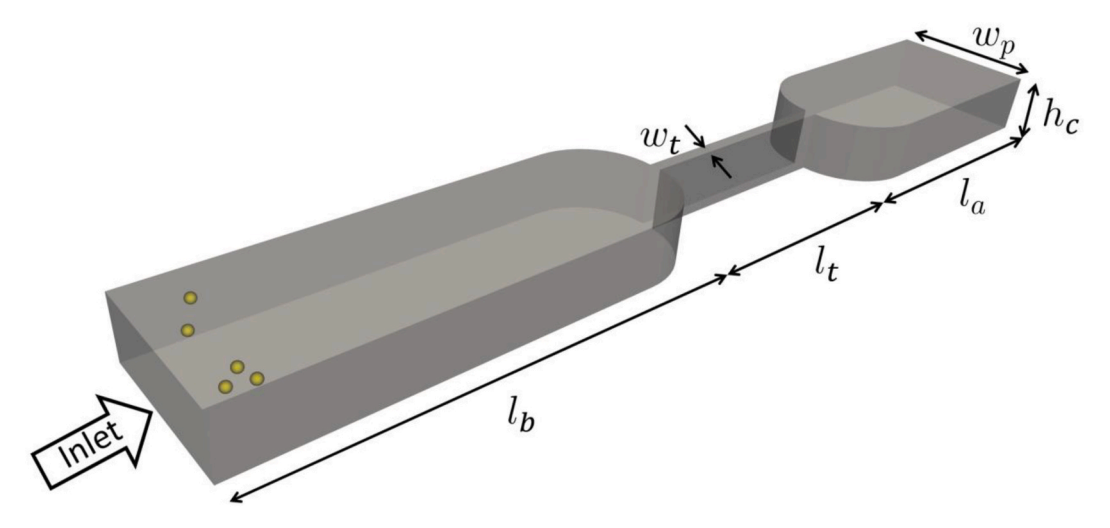


Fig. 2. 3D demonstration of the simulation domain.

Table 2Geometry parameters used in the simulations.

Property	Value (μm)
Before throat length, l_b	300
After throat length, l_a	200
Channel width, w_c	100
Channel height, hc	40
Throat width, w_t	10
Throat length, l_t	150

Table 3 Properties of fluids used in the simulations.

Property	Value
Fluid Density (kg/m^3)	1000
Fluid kinematic viscosity (m^2/s)	$1 imes10^{-6}$
CFD Time step (s)	$1 imes 10^{-3}$

Table 4Properties of particles used in the simulations.

Property	Value
Poisson's ratio	0.4
Friction Coefficient	0.5
Restitution Coefficient	0.3
Density (kg/m^3)	1000
Diameter (µm)	6
DEM time step (s)	$1 imes 10^{-5}$

Table 5Injection rates for different cases studied in this work.

Case	Injection Rate (μm_{S})	Case	Injection Rate (μm_{S})
Case #1	0.12	Case #6	0.42
Case #2	0.18	Case #7	0.48
Case #3	0.24	Case #8	0.54
Case #4	0.3	Case #9	0.6
Case #5	0.36	Case #10	1.2

within the throat but also in other regions of the domain, indicating that the DLVO considerations can influence the migration of fine particles even outside the throat. As such, the DLVO theory has the potential to significantly impact the particle distribution in the system. Furthermore, particle accumulation can be seen in Fig. 3 (e), which results in lower permeability of the system and consequently less energy for extraction (i.e., production), which is not desirable in such applications. However, permeability reduction is the goal of some applications, such as $\rm CO_2$ sequestration.

After demonstrating the influence of the existence of the DLVO force in the same injection rate, the effect of the injection rate on the clogging is illustrated in Fig. 4. Fig. 4 presents the impact of the injection rate on the occurrence of clogging. The results indicate that clogging can be avoided by using a higher injection rate, as observed in Case #10. In this scenario, the significant aggregation of particles, which is commonly observed in other cases, is not detected. This is because the fluid force at higher injection rates is able to overcome the bonding between particles, preventing the formation of large aggregates. Although some aggregation can still be seen in the domain, as shown in Fig. 4 (d), it is not sufficient to block the channel or throat since the fluid force is capable of breaking the particle bonding. This observation can also be interpreted as a change in the permeability of the domain. The number of particles at a lower injection rate is greater than the high injection rate; thus, the domain manifests a higher permeability at a higher injection rate; see Fig. 4.

As discussed, the clogging process can be initiated with the accumulation of just two particles. If the bonding between particles is strong enough or the fluid cannot break it, the particle aggregation can lead to throat clogging. Once particles form aggregations, the fluid attempts to break the particle bonds and clusters. When the fluid fails to break the accumulations, it adjusts its flow pattern to accommodate the presence of these clusters. Analyzing the fluid velocity field is, therefore, valuable in understanding the fluid behavior in such conditions. Fig. 5 illustrates the time evolution of the fluid velocity field and its interaction with particle aggregation. The impact of small aggregations in the early injection steps can be observed in Fig. 5(a) and (b). As expected, Fig. 5(a) shows a concentration of flow near the throat. However, the velocity field changes when particles accumulate near the throat, as depicted in Fig. 5(b). This indicates that the fluid becomes trapped behind the particle aggregation, resulting in a decrease in fluid velocity within the particle clusters and a modification of the flow pattern. This behavior is further exemplified in Fig. 5(c) and (d), where the fluid adapts to the presence of a large particle cluster after the throat. The fluid flow adjusts to navigate around the cluster, causing changes in the velocity field and flow pattern. The accurate capture of fluid adaptation demonstrates the effectiveness of the implemented CFD-DEM coupling in capturing fluidparticle interactions. This observation is also in line with our previous results regarding permeability changes. As can be seen in Fig. 5, in particle accumulation areas, the fluid velocity is considerably lower,

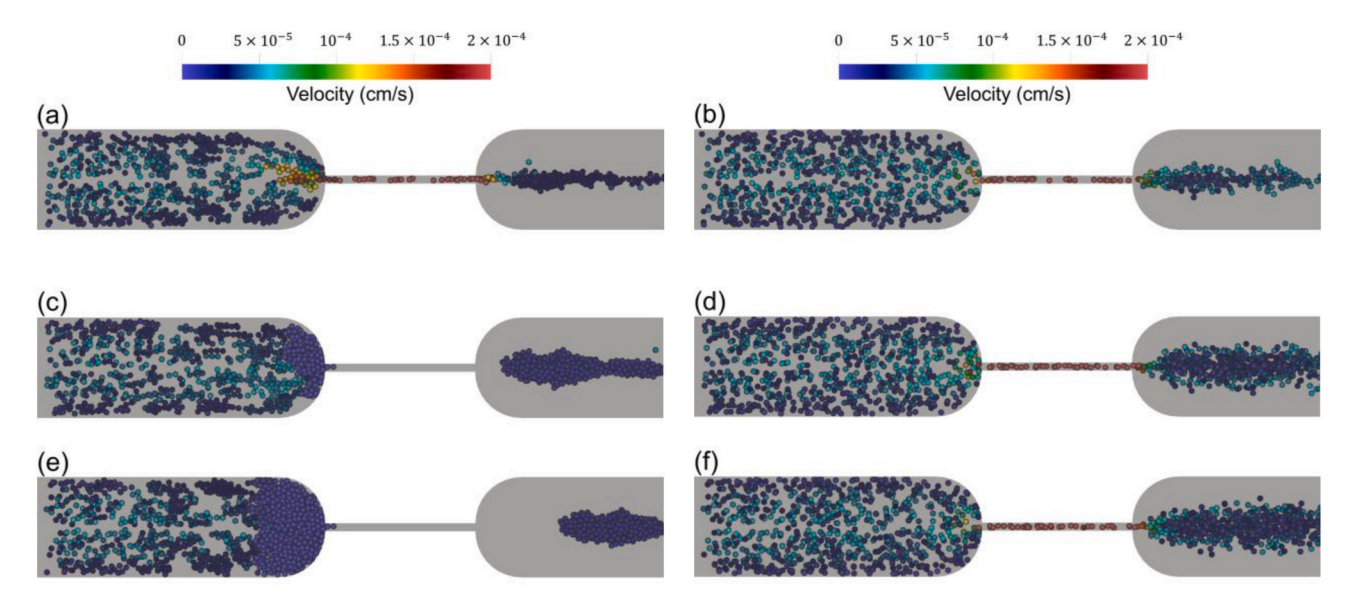


Fig. 3. Time evolution of fine particle movement during simulation for Case #5 at (a) t = 1000s with considering DLVO, (b) t = 1000s without considering DLVO, (c) t = 1500s with considering DLVO, (d) t = 1500s without considering DLVO, (e) t = 2000s with considering DLVO, (f) t = 2000s without considering DLVO.

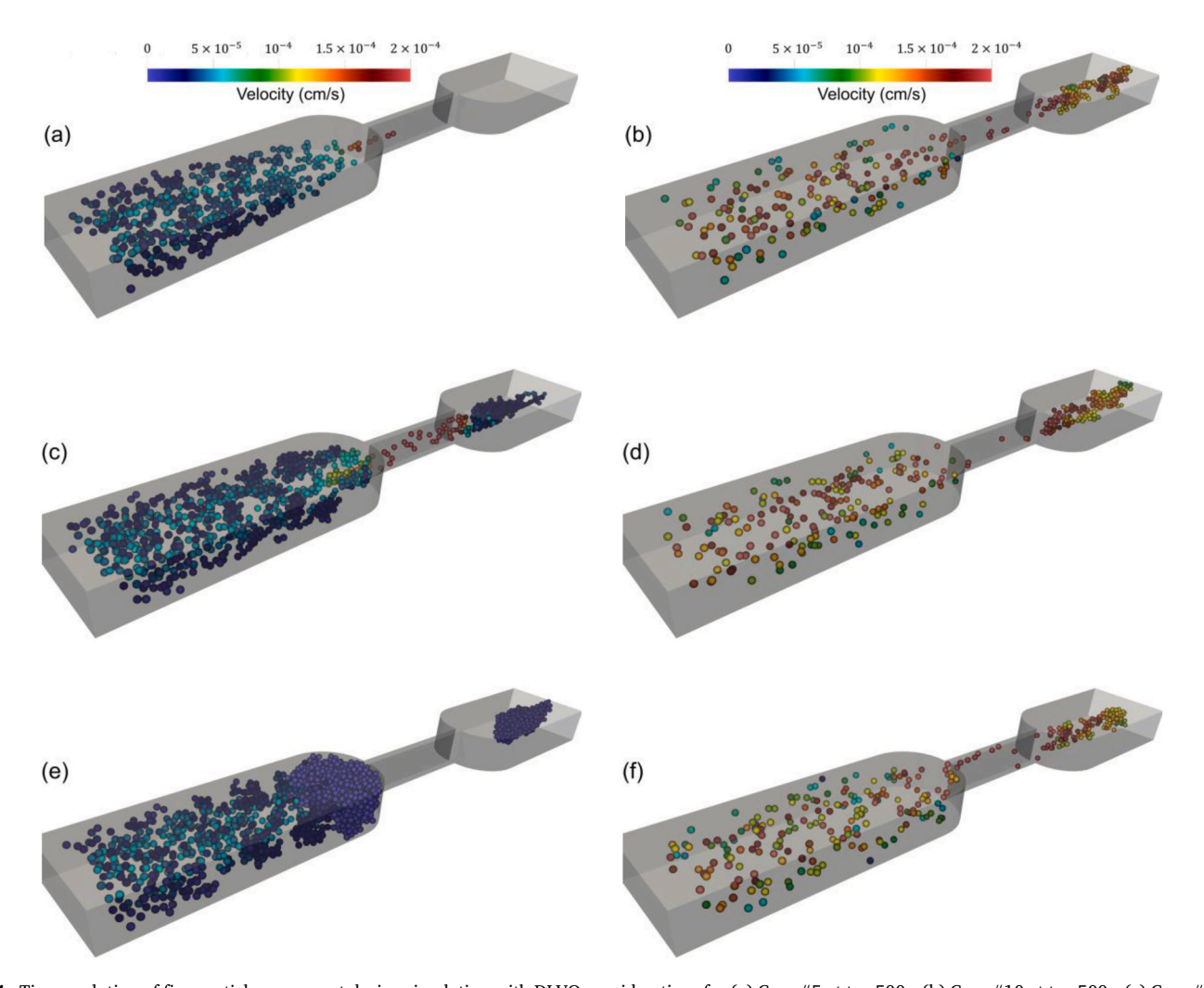


Fig. 4. Time evolution of fine particle movement during simulation with DLVO considerations for (a) Case #5 at t = 500s, (b) Case #10 at t = 500s, (c) Case #5 at t = 1000s, (d) Case #10 at t = 1000s, (e) Case #5 at t = 2000s, and (f) for Case #10 at t = 2000s. It is important to note that although the same number of particles is injected in each time interval for all cases, the presence of clogging results in a higher concentration of particles at specific time steps in the right column. However, the presented results on the right side show a lower accumulation of particles due to the absence of dominant clogging.

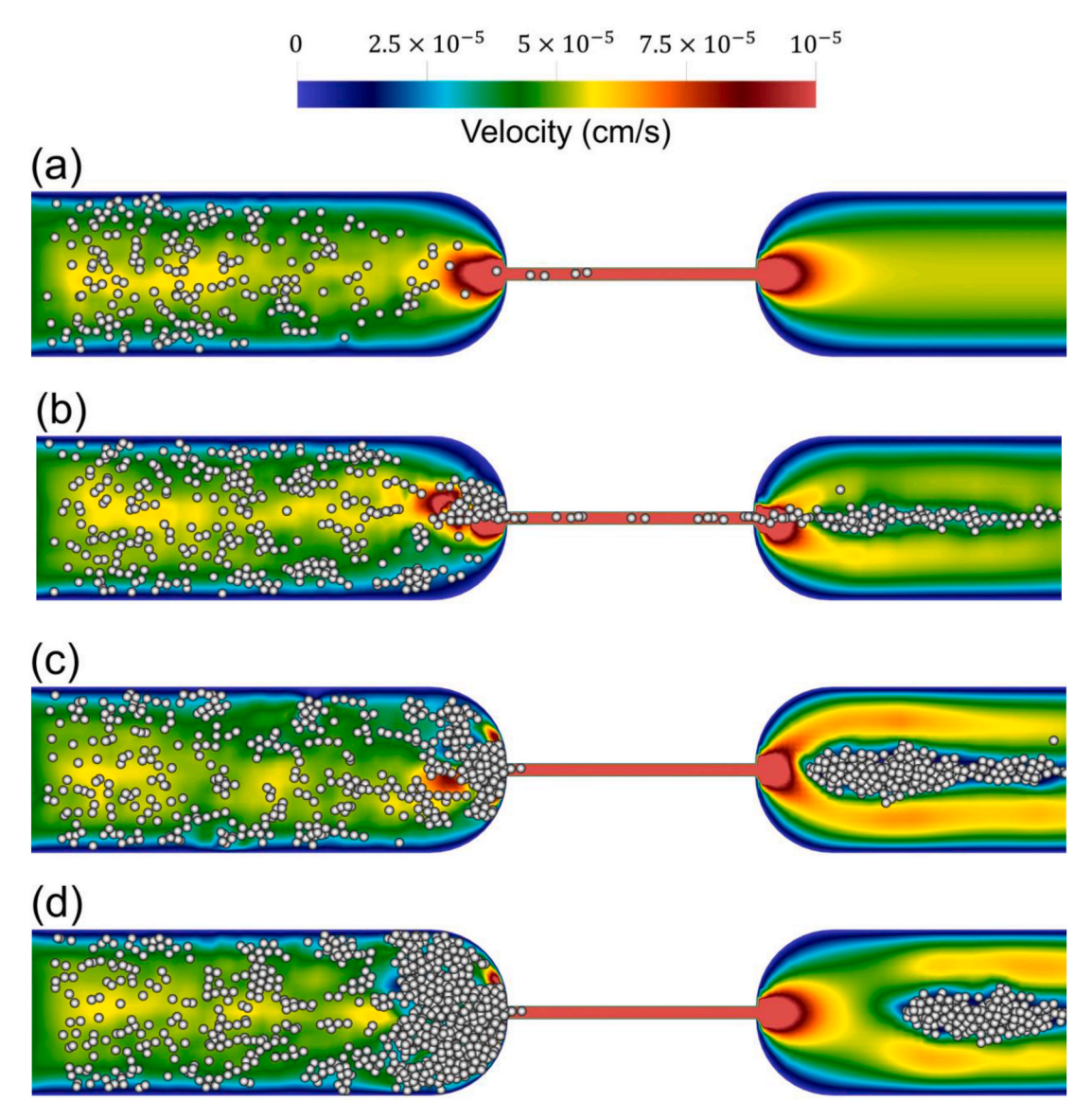


Fig. 5. Time evolution of fine particle movement during simulation considering DLVO theory for Case #5 at (a) t = 500s, (b) t = 1000s, (c) t = 1500s, and (d) t = 2000s

which means the fluid cannot freely travel. In other words, dropping permeability and porosity of the domain is inevitable in the clogging cases.

In order to quantify the findings regarding the influence of DLVO and injection rate on clogging, it is important to examine the particle concentration in different regions of the domain (i.e., before, after, and the domain). Fig. 6 illustrates the particle concentration in the domain. The results indicate that considering the DLVO force leads to an increase in the number of particles in the domain, although this increase is less pronounced for low injection rates (such as Case #1) and high injection rates (such as Case #10). This trend can be attributed to two reasons: 1) In low injection rate scenarios, the drag force applied to the particles is insufficient to move them effectively within the system, resulting in a higher particle concentration. 2) In high injection rate scenarios, the fluid flow is strong enough to break the bonding between particles and prevent them from forming large aggregations. This reduces the particle concentration in the domain. Furthermore, simulations without considering the DLVO force demonstrate an inverse relationship between injection rate and particle concentration in the domain. However, this relationship is not observed in cases where DLVO force is considered. Among all the cases, Case #4 exhibits the most significant change in particle concentration. Based on the results, clogging occurs for injection rates lower than that of Case #7, while no blockage is observed for Cases #7, #8, #9, and #10. Therefore, Case #6 is identified as the critical injection rate at which clogging can be expected. Additionally, the data in Fig. 6 supports our previous observations regarding the decrease in the porosity and permeability of the domain since the particle concentrations have an inverse relationship with porosity and permeability. To further support the claim regarding the critical injection rate, Figs. 7 and 8 depict the particle motion for Case #6 and Case #7, respectively. A comparison between these figures reinforces the assertion regarding the critical injection rate and its influence on the clogging process.

Fig. 9 presents the particle concentration before the throat, which is the region where clogging occurs and obstructs the flow passage. The analysis of particle concentration in this region provides further insights into the clogging phenomenon. In non-DLVO cases presented in Fig. 9 (b)—a clear inverse relationship is observed between the injection rate and particle concentration before the throat. As the injection rate increases, the particle concentration decreases, indicating that higher flow rates prevent significant particle accumulations in this region. Fig. 9(a) demonstrates two distinct regions: non-clogging and clogging regions. In

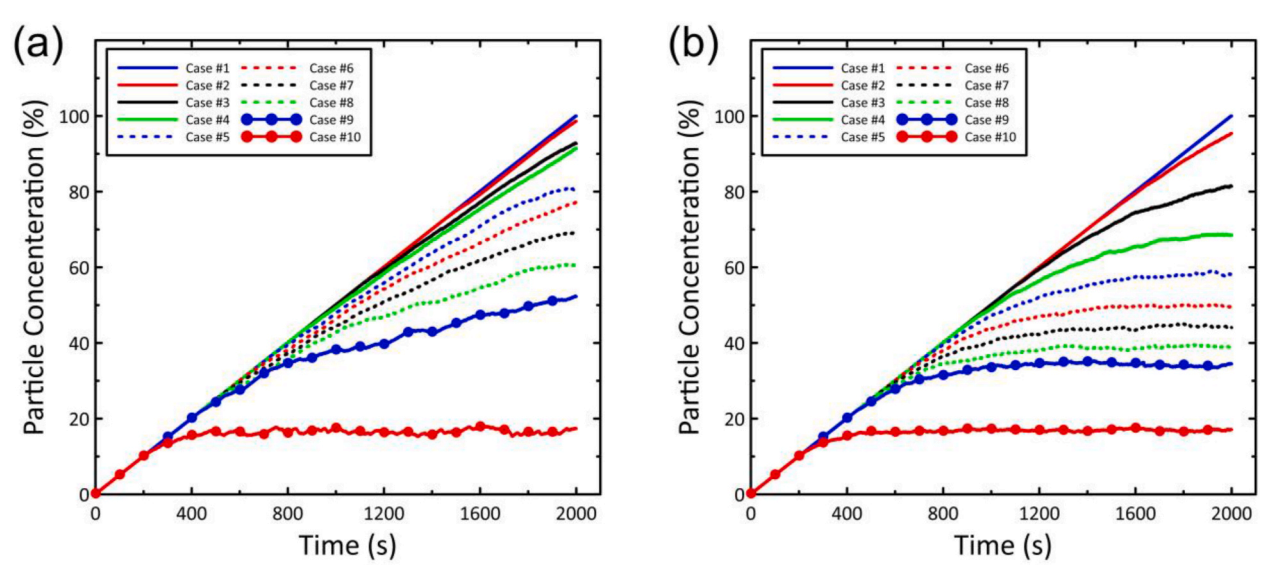


Fig. 6. Time evolution of particle concentration in the domain during simulation (a) considering DLVO theory and (b) without DLVO force between particles.

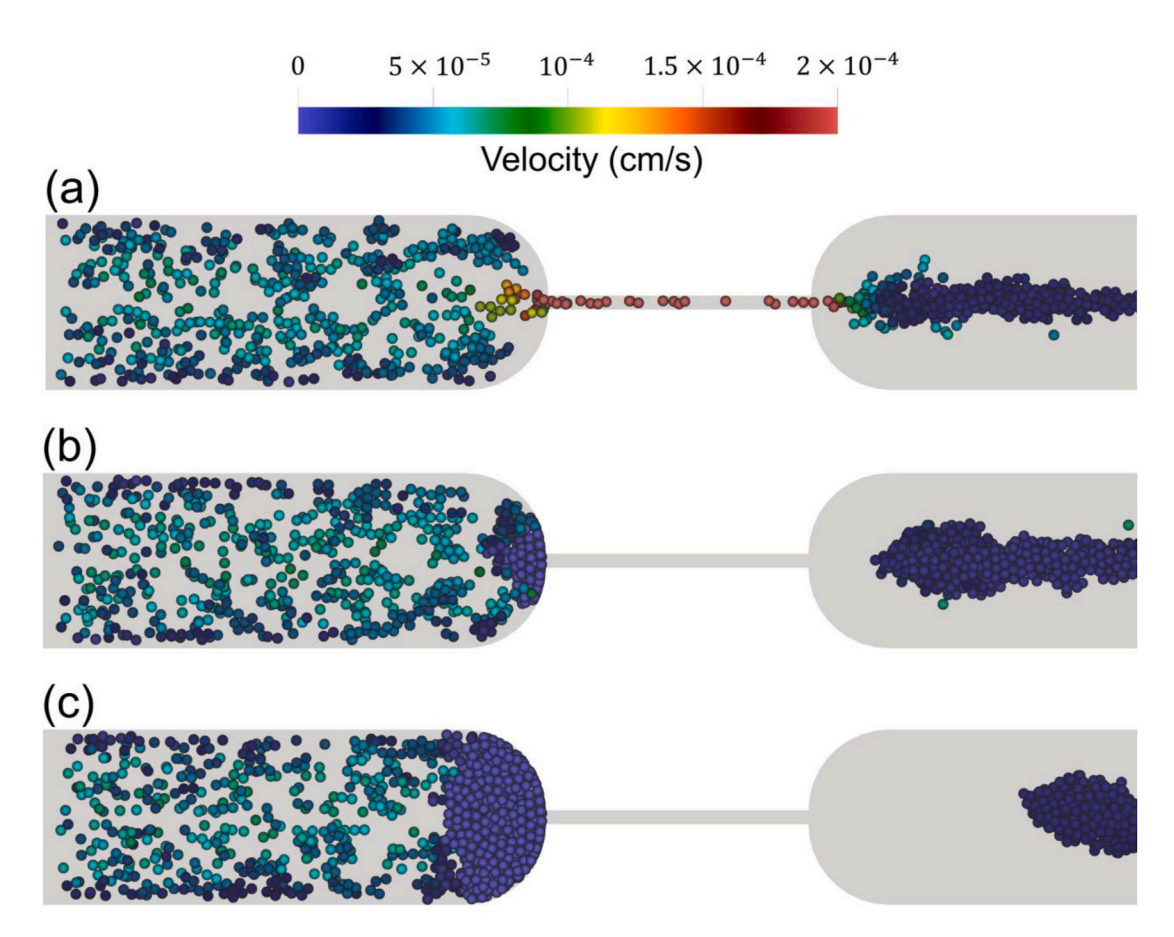


Fig. 7. Time evolution of fine particle motions in the domain for Case #6 at (a) t = 500s, (b) t = 1500s, (c) t = 2000s.

the non-clogging region, the injection rates are greater than that of Case #6, while in the clogging region, the injection rate is lower than that of Case #7. This observation further supports the identification of Case #6 as the critical injection rate where clogging is expected to occur. Moreover, our results indicate that in DLVO cases, approximately 80% of the injected particles are positioned before the throat at low injection rates by the end of the simulations. This suggests a significant accumulation of particles in this region due to the influence of DLVO forces.

Thus, this area has considerably less porosity, which indicates that the fluid cannot move as freely as before in such areas (i.e., lower permeability). Interestingly, in high inlet velocity cases (Case #7 to Case #10), the particle concentration before the throat shows minimal variation between DLVO and non-DLVO cases. This indicates that the impact of DLVO considerations becomes less pronounced in scenarios with higher flow rates. The difference between DLVO and non-DLVO cases can be attributed to the formation of small aggregations in the presence of

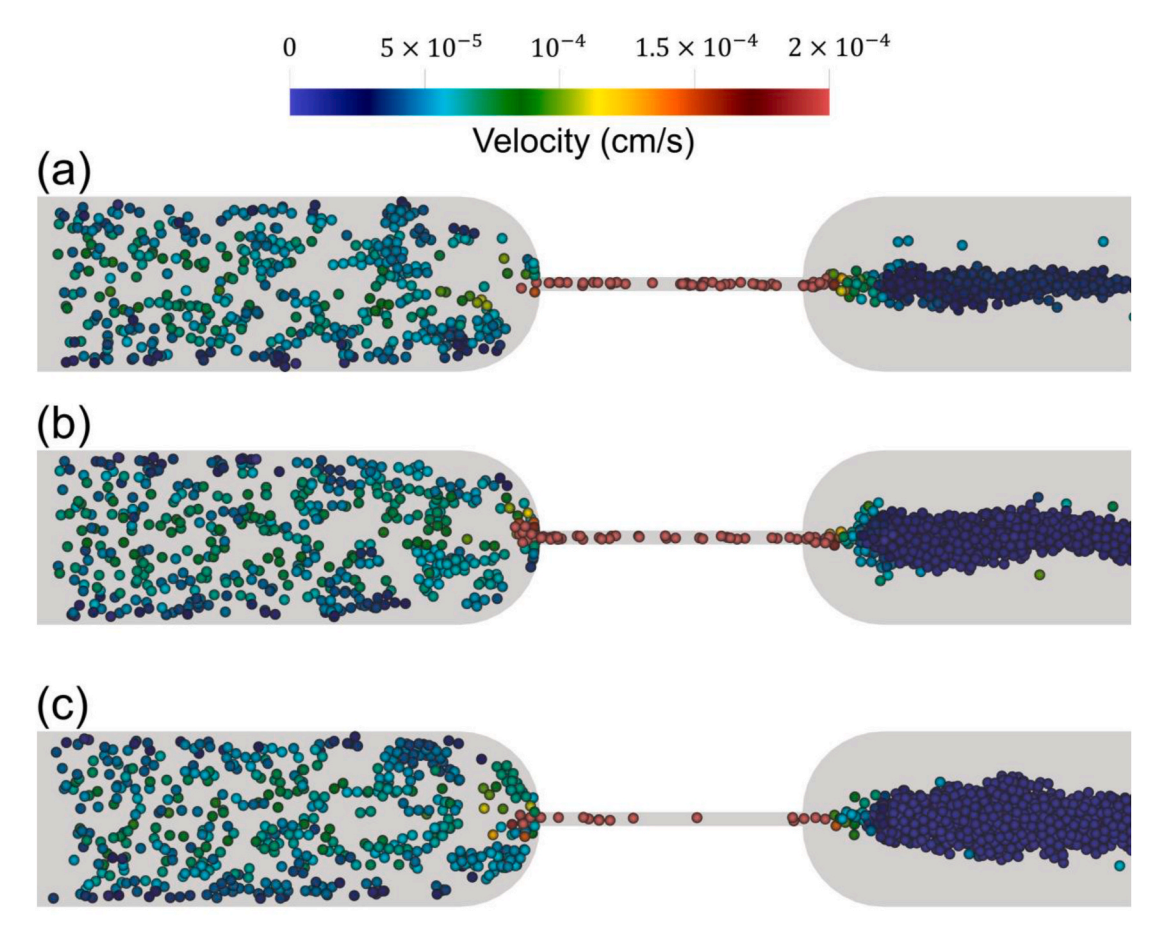


Fig. 8. Time evolution of fine particle motions in the domain for Case #7 at (a) t = 500s, (b) t = 1500s, (c) t = 2000s.

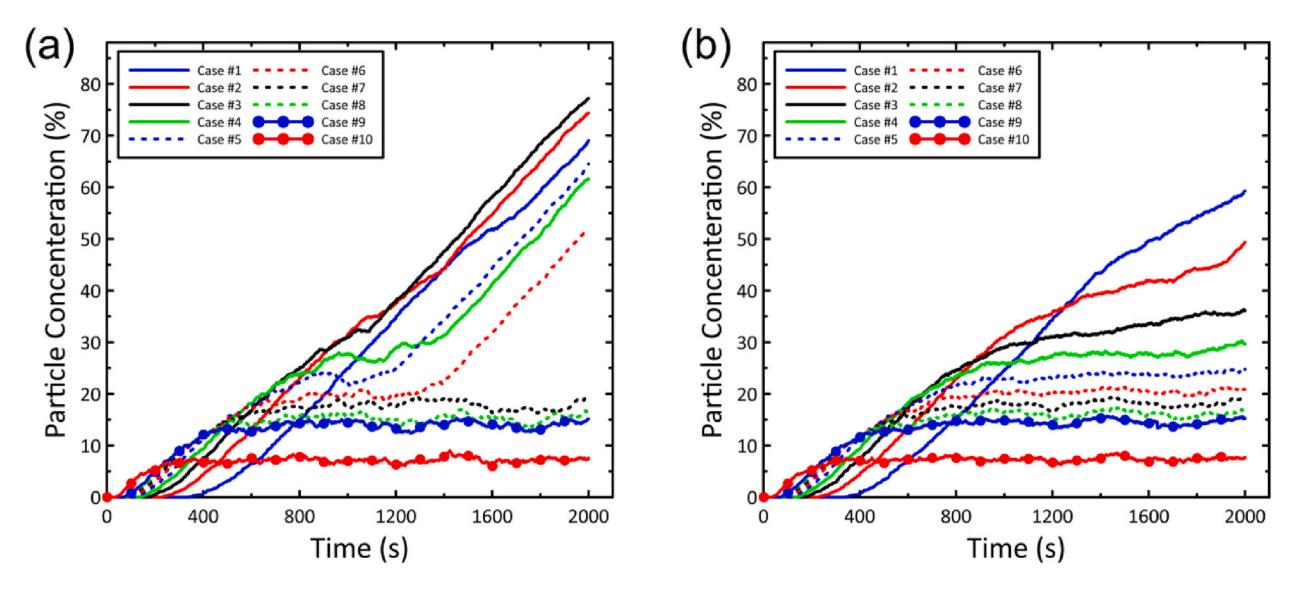


Fig. 9. Time evolution of particle concentration before the throat during simulation (a) considering DLVO theory and (b) without DLVO force between particles.

DLVO forces.

To complete our understanding of the impact of the DLVO and injection rate in clogging, we need to analyze the number of particles after the throat. To this end, Fig. 10 is demonstrated. In DLVO cases, the highest particle concentration after the throat is observed in Case #7 to Case #9. In these cases, particle agglomerations are formed either before or after the throat, but the fluid force prevents them from becoming large enough to block the throat. This indicates that the DLVO forces

play a significant role in particle aggregation, but the fluid force counteracts their effect to some extent. Noticeably, the impact of DLVO forces is minimized in Case #10. Our findings show that in Case #10, only small aggregations (consisting of a couple of particles) remain in the domain due to the powerful fluid force. Therefore, as the injection rate increases, the size of aggregates decreases. On the other hand, the number of particles in lower injection rate cases (Case #1 to Case #6) decreases significantly when DLVO forces are considered. In other

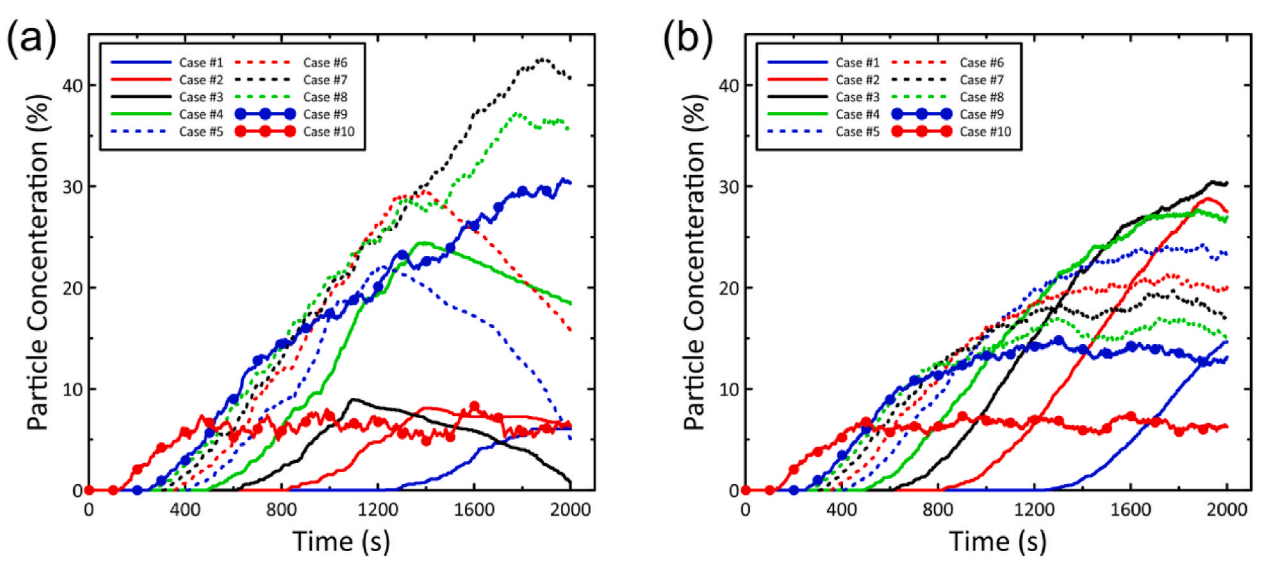


Fig. 10. Time evolution of particle concentration after the throat during simulation (a) considering DLVO theory and (b) without DLVO force between particles.

words, the DLVO theory not only affects the porosity before the throat areas but also impacts the area after throat. Thus, the presence of DLVO forces affects both the particle motion before and after the throat.

After quantifying the number of particles in different regions in the domain and their influence, one should study the DLVO impact on fluidparticle and particle-particle forces. To do so, the fluid-particle force (i. e., Drag force) is presented in Fig. 11. A comparison between Fig. 11(a) and (b) reveals that considering DLVO forces at least doubles the drag force. This indicates that DLVO forces have a significant effect on the interaction between the fluid and particles, even in cases with higher injection rates where throat clogging does not occur. In non-DLVO cases, the drag force increases with higher fluid injection velocities, which is expected due to the increased flow momentum. However, the presence of DLVO forces changes this trend. For example, in Case #6, the average drag force is six times higher when DLVO forces are considered compared to the non-DLVO case. This significant difference is solely attributed to the presence of particle clusters. Each cluster consists of particles that are bonded together, resulting in an increased contact area between the cluster and the fluid. Also, the fluid flow gets obstructed by the cluster, requiring a higher force to push it, leading to a greater drag

force. These findings highlight the importance of DLVO forces in modifying the fluid-particle interactions and the resulting drag forces. It also demonstrates that particle clustering, facilitated by DLVO forces, has a significant impact on the overall fluid-particle dynamics.

The other parameter in which the DLVO influence can be seen is the inter-particle force. Fig. 12 demonstrates the inter-particle force and allows us to examine the influence of DLVO forces on this parameter. Comparing Fig. 12(a) and (b), it is clear that considering DLVO forces increases the inter-particle force. The DLVO force effectively keeps particles closer together, resulting in a higher number of particles in contact with each other. As a result, the inter-particle force is increased. This observation highlights the role of DLVO forces in promoting particle clustering and the subsequent increase in inter-particle forces. The highest values of inter-particle force are observed in cases with lower injection rates. In these scenarios, the inter-particle force dominates over the fluid-particle forces. Furthermore, Fig. 12(b) demonstrates that the injection rate also affects the inter-particle force in non-DLVO cases. In simulations without DLVO forces, as the injection rate (or fluid velocity) increases, the particle velocity also increases, leading to greater forces during particle collisions.

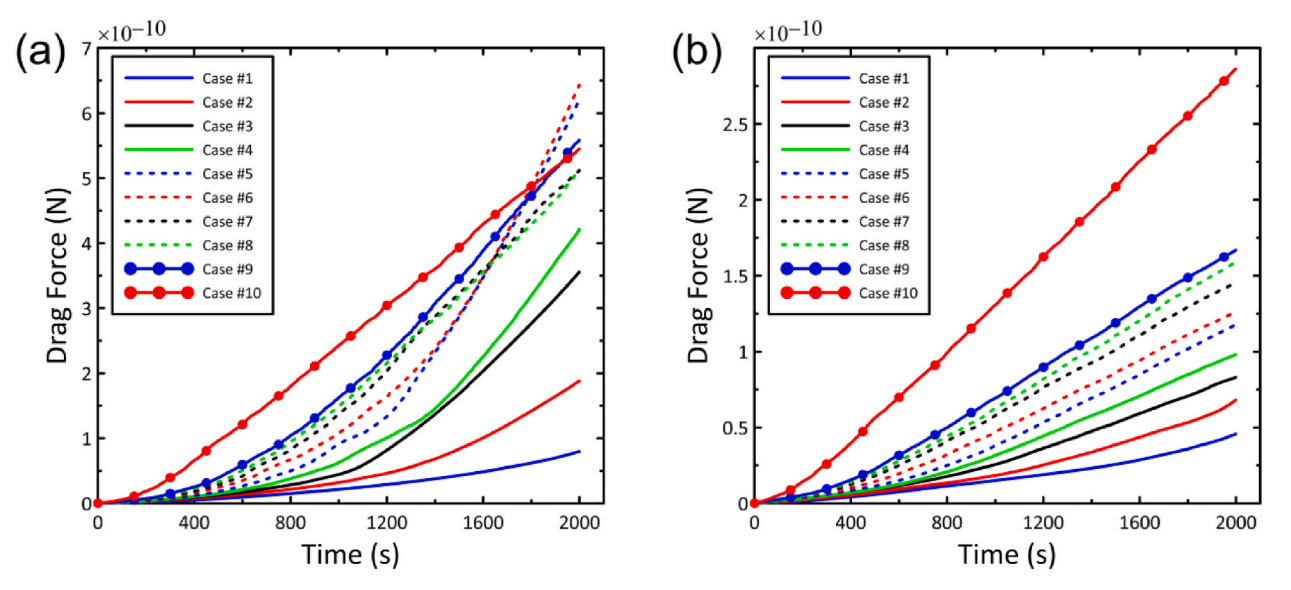


Fig. 11. Time evolution of the average drag force in the domain during simulation (a) considering DLVO theory and (b) without DLVO force between particles.

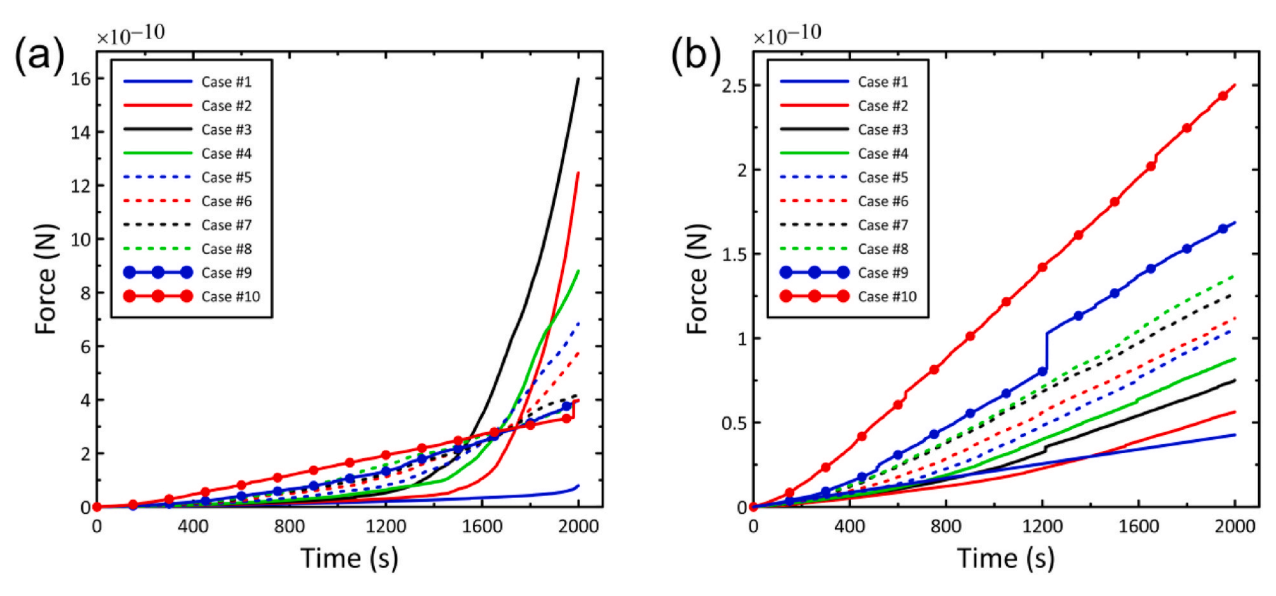


Fig. 12. Time evolution of the average inter-particle force in the domain during simulation (a) considering DLVO theory and (b) without DLVO force between particles.

The analysis of particle velocities, specifically the translational and rotational velocities, provides valuable insights into the behavior of particles. Figs. 13 and 14 illustrate the comparison between DLVO and non-DLVO cases. The analysis reveals that the difference in translational velocity between DLVO and non-DLVO cases is relatively small. However, it is worth noting that after the particles block the channel (i.e., Time >800 s), both the translational and rotational velocities decrease. This decrease can be attributed to the hindered movement caused by the presence of particle aggregates. On the other hand, a significant difference is observed in the angular velocity between DLVO and non-DLVO cases. In DLVO simulations, where particle aggregation occurs, the rotational motion of individual particles within the aggregates is limited due to the inter-particle forces. As a result, the angular velocity decreases considerably compared to non-DLVO cases. These findings emphasize the role of DLVO forces in promoting particle aggregation and reducing the rotational motion of particles within the aggregates. The limitation of particle rotations within aggregates further contributes to the overall behavior and dynamics of the clogging process.

Time (s)

The effect of injection rate and the DLVO force on the fluid velocity is analyzed through the calculation of the dimensionless average fluid velocity difference, denoted as V_f^* in Fig. 15. The results indicate that lower injection rates, which are associated with higher clogging rates (as shown in Figs. 6, 9 and 10), exhibit approximately a 12% velocity difference between DLVO and non-DLVO cases. This decreasing trend in the average velocity supports our previous discussion on the influence of the DLVO on the porosity and permeability of the system at each injection rate. On the other hand, higher injection rate cases demonstrate the lowest velocity difference. This implies that the inclusion of the DLVO force, which represents particleparticle interactions, has an impact on the fluid velocity even when the injection rate remains the same since the permeability of the system is dropping in cases where we had clogging. The observed transition from low injection rates to high injection rates further supports this finding.

Finally, the other quantity of interest is the momentum exchange,

 M^{f-p} in Eq. (8). To understand the influence of injection rate and DLVO

Time (s)

(a) (b) Velocity (cm/s) Velocity (cm/s) 0.5 0.5 0 400 1200 1600 400 800 1200 2000 0 2000 0 1600

Fig. 13. Time evolution of the average transitional velocity in the domain during simulation (a) considering DLVO theory and (b) without DLVO force between particles.

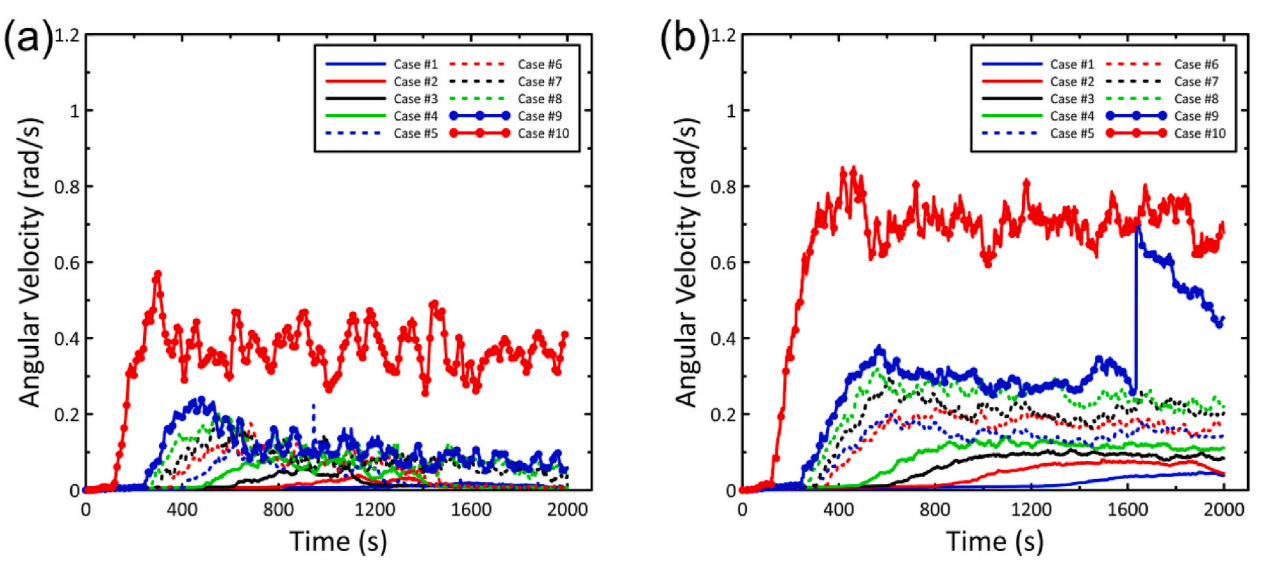


Fig. 14. Time evolution of the average rotational velocity in the domain during simulation (a) considering DLVO theory and (b) without DLVO force between particles.

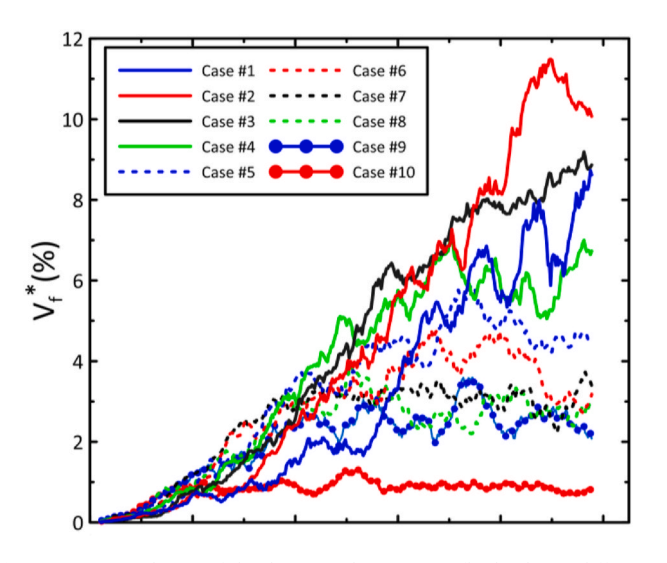
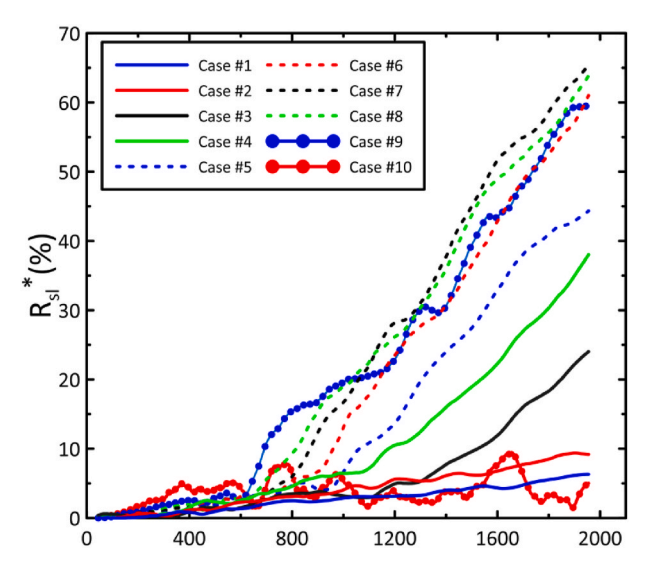


Fig. 15. Time evolution of the dimensionless average fluid velocity difference in the domain during simulation.

force simultaneously, the normalized momentum exchange $(R_{sl}^* = \left| \frac{R_{sl}^{\text{DUVO}} - R_{sl}^{\text{mom-DLVO}}}{R_{sl}^{\text{mom-DLVO}}} \right|)$ is illustrated in Fig. 16. The results demonstrate that, even with the same injection rate, there are differences in both fluid velocity (as shown in Figs. 15 and 16) and momentum exchange. This discrepancy can be attributed to the presence of particle aggregations in the DLVO cases. Although these aggregations are not large enough to completely block the throat in high injection rate scenarios, they still contribute to a significant difference in momentum exchange. The influence of these small aggregations is more prominent in cases with higher injection rates, such as Case #7. Furthermore, it is worth noting that there is a substantial difference of over 60% in the momentum exchange for Case #6, which corresponds to the critical injection rate. This emphasizes the critical role of injection rate and the presence of particle aggregations in determining the momentum exchange and overall fluid-particle interaction.

To sum up, we studied the inter-particle forces, fluid-particle forces, particle velocity (linear and angular), fluid velocity, and momentum exchange. In all mentioned parameters, one can observe the influence of the DLVO and injection rate. In energy applications, the occurrence of



 $\begin{tabular}{ll} {\bf Fig.~16.} & {\bf Time~evolution~of~the~normalized~momentum~exchange~in~the~domain~during~simulation.} \end{tabular}$

clogging has been considered as a key phenomenon since it can considerably change the porosity and permeability of the system. Also, as discussed, the application can define if the clogging is desirable or unwilling. For instance, in the energy production procedure in geothermal and hydrogen storage systems, clogging leads to a considerable decrease in the permeability of the domain, which is undesirable. On the other hand, clogging is viewed as a desirable feature for carbon storage. Hence, we introduced a critical injection rate, given the considered boundary conditions, where we did not observe any clogging when the velocity exceeded a threshold (i.e., critical injection rate) even with DLVO considerations. Furthermore, observed changes in average velocity and momentum exchange between DLVO and non-DLVO cases (i.e., Figs. 15 and 16) showed how flow rate in the energy production and storage applications can be affected by the clogging occurrence.

5. Summary and conclusions

The primary objectives of this study were to investigate the effects of DLVO theory consideration and injection rate on the clogging phe-

nomenon at the microscale. In order to capture the intricate particleparticle and particle-fluid interactions inherent in such a system, we employed a CFD-DEM coupling approach and incorporated the DLVO theory in our numerical simulations. For our study, we conducted a series of 20 simulations, employing 10 different injection rates within the domain. By analyzing the particle behavior in various regions of the domain, we aimed to assess the impact of the DLVO theory and injection rate on clogging. To provide a quantitative analysis of our findings, we examined key factors such as particle-particle forces, fluid-particle forces (specifically, drag forces), transitional velocity, angular velocity, as well as the differences between DLVO and non-DLVO cases in terms of momentum exchange and fluid velocity. By systematically investigating these aspects, we aimed to gain a comprehensive understanding of how the DLVO theory and injection rate influence clogging processes at the microscale. The main findings of this paper can be summarized as follows.

- The comparison between DLVO and non-DLVO cases showed us that the DLVO consideration in such systems can cause blockage (i.e., clogging).
- 2. The aggregation of particles is the main reason for clogging. However, we observed particle aggregations cannot block the throat in some cases (i.e., high injection rates) since they are not big enough. Hence, the size of the particle cluster matters in the clogging process.
- In non-DLVO scenarios, with the increase of the injection rate, the drag force, inter-particle force, transitional velocity, and rotational velocity increases. However, after considering the DLVO theory, the mentioned relation was not observed.
- 4. In DLVO cases, the clear transition between injection rates was observed to have or avoid clogging in the domain. To be more specific, we found the critical injection rate, where a slight increase in the injection rate (i.e., $0.06\mu m/s$) can prevent clogging.
- The influence of the DLVO consideration in the fluid and particle behavior was observed even in scenarios where clogging did not happen. For instance, the drag force doubled for the non-clogging simulations.
- 6. Particle concentration analysis in different regions of the domain showed us that DLVO considerations decrease the porosity of the domain (i.e., the higher number of particles means lower porosity). As a result, lower porosity leads to lower void space, and since the injection rate is the same in DLVO and non-DLVO cases, it means lower permeability.
- 7. The rotational velocity is more affected by the DLVO considerations than transitional velocity because a particle can rotate easier than the accumulation of particles.

Thus, to understand the fluid and particle behavior in fine particle migration and study the clogging process, one should consider the DLVO theory due to its impact. Furthermore, the proposed CFD-DEM coupling can be considered a reliable solution to model the clogging process and fulfill one's needs concerning the blockage on such a scale. Also, our findings highlighted the influence of injection rate where after a small change in the injection rate (i.e., $\pm 0.06 \, \mu m/s$), one can prevent or ease the clogging. So, numerical and/or experimental studies can be conducted with DLVO consideration for future studies. Our study is limited to different injection rates; however, future studies might study the influence of different fluid viscosity and thermodynamic considerations. Although previous investigations showed that the shape of particles can influence the behavior of particle systems, our simulations rely on spherical particles. Hence, future studies can be focused on the irregular shape of particles in such a scale to consider the influence of particle's shape in the clogging (Amir Hosseini and Tahmasebi, 2023; Tahmasebi, 2019; Zhang and Tahmasebi, 2022, 2023). Furthermore, the impact of surface roughness is neglected in this work, which can be investigated in future studies. One might also consider the effects of different throat and domain sizes to draw a more comprehensive conclusion for the proposed

method in this paper.

CRediT authorship contribution statement

Mehryar Amir Hosseini: Writing – original draft, Visualization, Investigation, Formal analysis, Data curation. **Pejman Tahmasebi:** Writing – review & editing, Supervision, Resources, Project administration, Methodology, Investigation, Funding acquisition, Conceptualization.

Declaration of competing interest

The authors declare that they have no known competing financial interests or personal relationships that could have appeared to influence the work reported in this paper.

Data availability

Data will be made available on request.

Acknowledgments

The author would like to thank the financial support from the Colorado School of Mines for this research. This study was also supported by NSF (Grant #CMMI-2000966).

References

- Agbangla, G.C., Bacchin, P., Climent, E., 2014. Collective dynamics of flowing colloids during pore clogging. Soft Matter 10, 6303–6315. https://doi.org/10.1039/ CASNOSCOC
- Amir Hosseini, M., Kamrava, S., Sahimi, M., Tahmasebi, P., 2023. Effect of Wettability on two-phase flow through granular porous media: fluid rupture and mechanics of the media. Chem. Eng. Sci. 269, 118446 https://doi.org/10.1016/J.CES.2023.118446.
- Amir Hosseini, M., Tahmasebi, P., 2023. On the influence of the natural shape of particles in multiphase fluid systems: granular collapses. Comput. Geotech. 162, 105654 https://doi.org/10.1016/j.compgeo.2023.105654.
- Bacchin, P., Derekx, Q., Veyret, D., Glucina, K., Moulin, P., 2014. Clogging of microporous channels networks: role of connectivity and tortuosity. Microfluid. Nanofluidics 17, 85–96. https://doi.org/10.1007/S10404-013-1288-4/FIGURES/13.
- Bagheri, M., Shariatipour, S.M., Ganjian, E., 2019. Prediction of the lifespan of cement at a specific depth based on the coupling of geomechanical and geochemical processes for CO2 storage. Int. J. Greenh. Gas Control 86, 43–65. https://doi.org/10.1016/J. LJGGC.2019.04.016.
- Baiyu, Z., Hongming, T., Senlin, Y., Gongyang, C., Feng, Z., Shiyu, X., 2021. Effect of fracture roughness on transport of suspended particles in fracture during drilling. J. Pet. Sci. Eng. 207, 109080 https://doi.org/10.1016/J.PETROL.2021.109080.
- Baker, M.C., Kong, B., Capecelatro, J., Desjardins, O., Fox, R.O., 2020. Direct comparison of Eulerian–Eulerian and Eulerian–Lagrangian simulations for particle-laden vertical channel flow. AIChE J. 66, e16230 https://doi.org/10.1002/aic.16230.
- Berthet, H., Fermigier, M., Lindner, A., 2013. Single fiber transport in a confined channel: microfluidic experiments and numerical study. Phys. Fluids 25, 103601. https://doi.org/10.1063/1.4823728/258929.
- Cao, S.C., Jang, J., Jung, J., Waite, W.F., Collett, T.S., Kumar, P., 2019. 2D micromodel study of clogging behavior of fine-grained particles associated with gas hydrate production in NGHP-02 gas hydrate reservoir sediments. Mar. Petrol. Geol. 108, 714-730. https://doi.org/10.1016/J.MARPETGE0.2018.09.010.
- Cui, G., Ning, F., Dou, B., Li, T., Zhou, Q., 2022. Particle migration and formation damage during geothermal exploitation from weakly consolidated sandstone reservoirs via water and CO2 recycling. Energy 240, 122507. https://doi.org/ 10.1016/J.ENERGY.2021.122507.
- Cundall, P.A., Strack, O.D.L.L., 1979. A discrete numerical model for granular assemblies. Geotechnique 29, 47–65. https://doi.org/10.1680/geot.1979.29.1.47.
- Daigle, H., Cook, A., Fang, Y., Bihani, A., Song, W., Flemings, P.B., 2020. Gas-Driven tensile fracturing in shallow marine sediments. J. Geophys. Res. Solid Earth 125, e2020JB020835. https://doi.org/10.1029/2020JB020835.
- Dalla Vecchia, F., Dos Santos, V.H.J.M., Schütz, M.K., Ponzi, G.G.D., Stepanha, A.S. de G. e., Malfatti, C. de F., Costa, E.M. da, 2020. Wellbore integrity in a saline aquifer: experimental steel-cement interface degradation under supercritical CO2 conditions representative of Brazil's Parana basin. Int. J. Greenh. Gas Control 98, 103077. https://doi.org/10.1016/J.IJGGC.2020.103077.
- Di Vaira, N.J., Łaniewski-Wołłk, Ł., Johnson, R.L., Aminossadati, S.M., Leonardi, C.R., 2023. Hydrodynamic clogging of micro-particles in planar channels under electrostatic forces. J. Fluid Mech. 960, A34. https://doi.org/10.1017/ JFM.2023.214.

- Dincau, B., Tang, C., Dressaire, E., Sauret, A., 2022. Clog mitigation in a microfluidic array via pulsatile flows. Soft Matter 18, 1767–1778. https://doi.org/10.1039/ D2SM000131
- Divoux, T., Lapeyre, V., Ravaine, V., Manneville, S., 2015. Wall slip across the jamming transition of soft thermoresponsive particles. Phys. Rev. E - Stat. Nonlinear Soft Matter Phys. 92, 060301 https://doi.org/10.1103/PHYSREVE.92.060301/ EICHERS (AMEDIUM)
- Dressaire, E., Sauret, A., 2016. Clogging of microfluidic systems. Soft Matter 13, 37–48. https://doi.org/10.1039/C6SM01879C.
- Duru, P., Hallez, Y., 2015. A three-step scenario involved in particle capture on a pore edge. Langmuir 31, 8310–8317. https://doi.org/10.1021/ACS. LANGMUIR.5B01298/SUPPL_FILE/LA5B01298_SL_001.PDF.
- El Shamy, U., Sizkow, S.F., 2021. Coupled SPH-DEM simulations of liquefaction-induced flow failure. Soil Dynam. Earthq. Eng. 144, 106683 https://doi.org/10.1016/j.soildyn.2021.106683
- Elghannay, H., Tafti, D., 2018. LES-DEM simulations of sediment transport. Int. J. Sediment Res. 33, 137–148. https://doi.org/10.1016/j.ijsrc.2017.09.006.
- Ergun, S., 1952. Fluid flow through packed columns. Chem. Eng. Prog. 48, 89-94.
- Fang, B., Lü, T., Ning, F., Pang, J., He, Z., Sun, J., 2022. Facilitating gas hydrate dissociation kinetics and gas migration in clay interlayer by surface cations shielding effects. Fuel 318, 123576. https://doi.org/10.1016/J.FUEL.2022.123576.
- Gaol, C.L., Ganzer, L., Mukherjee, S., Alkan, H., 2021. Investigation of clogging in porous media induced by microorganisms using a microfluidic application. Environ. Sci. Water Res. Technol. 7, 441–454. https://doi.org/10.1039/D0EW00766H.
- Giglia, S., Straeffer, G., 2012. Combined mechanism fouling model and method for optimization of series microfiltration performance. J. Membr. Sci. 417–418, 144–153. https://doi.org/10.1016/J.MEMSCI.2012.06.026.
- Hamaker, H.C., 1937. The London—van der Waals attraction between spherical particles. Physica 4, 1058–1072. https://doi.org/10.1016/S0031-8914(37)80203-7.
- Han, Y., Cundall, P.A., 2013. LBM-DEM modeling of fluid-solid interaction in porous media. Int. J. Numer. Anal. Methods GeoMech. 37, 1391–1407.
- Henry, C., Minier, J.P., Lefèvre, G., 2012. Towards a description of particulate fouling: from single particle deposition to clogging. Adv. Colloid Interface Sci. 185–186, 34–76. https://doi.org/10.1016/J.CIS.2012.10.001.
- Hou, Q., Miao, C., Chen, S., Sun, Z., Karemat, A., 2023. A Lagrangian particle model on GPU for contaminant transport in groundwater. Comput. Part. Mech. 10, 587–601. https://doi.org/10.1007/S40571-022-00495-5/FIGURES/13.
- Huilin, L., Gidaspow, D., 2003. Hydrodynamics of binary fluidization in a riser: CFD simulation using two granular temperatures. Chem. Eng. Sci. 58, 3777–3792. https://doi.org/10.1016/S0009-2509(03)00238-0.
- Kang, W., Wang, J., Ye, Z., Gu, G., Li, W., Yang, H., Li, Z., Xu, H., Lv, Z., Sarsenbekuly, B., 2022. Study on preparation and plugging effect of sawdust gel particle in fractured reservoir. J. Pet. Sci. Eng. 212, 110358 https://doi.org/10.1016/J. PETROL.2022.110358.
- Kloss, C., Goniva, C., Hager, A., Amberger, S., Pirker, S., 2012. Models, algorithms and validation for opensource DEM and CFD-DEM. Prog. Comput. Fluid Dynam. Int. J. 12. 140–152. https://doi.org/10.1504/PCFD.2012.047457.
- Knight, C., O'Sullivan, C., van Wachem, B., Dini, D., 2020. Computing drag and interactions between fluid and polydisperse particles in saturated granular materials. Comput. Geotech. 117, 103210 https://doi.org/10.1016/J. COMPGEO.2019.103210.
- Lee, J. Le, Lim, E.W.C., 2017. Comparisons of Eulerian-Eulerian and CFD-DEM simulations of mixing behaviors in bubbling fluidized beds. Powder Technol. 318, 193–205. https://doi.org/10.1016/j.powtec.2017.05.050.
- Li, R., Li, G., Feng, Y., Yang, X., Teng, Y., Hu, Y., 2022. Innovative experimental method for particle bridging behaviors in natural fractures. J. Nat. Gas Sci. Eng. 97, 104379 https://doi.org/10.1016/J.JNGSE.2021.104379.
- Li, X., Zhao, J., 2018. Dam-break of mixtures consisting of non-Newtonian liquids and granular particles. Powder Technol. 338, 493–505. https://doi.org/10.1016/J. POWTEC.2018.07.021.
- Liang, Y., Tan, Y., Luo, Y., Zhang, Y., Li, B., 2020. Progress and challenges on gas production from natural gas hydrate-bearing sediment. J. Clean. Prod. 261, 121061 https://doi.org/10.1016/J.JCLEPRO.2020.121061.
- Lin, C., Taleghani, A.D., Kang, Y., Xu, C., 2022. A coupled CFD-DEM simulation of fracture sealing: effect of lost circulation material, drilling fluid and fracture conditions. Fuel 322, 124212. https://doi.org/10.1016/J.FUEL.2022.124212.
- Lin, Q., Akai, T., Blunt, M.J., Bijeljic, B., Iwama, H., Takabayashi, K., Onaka, Y., Yonebayashi, H., 2021. Pore-scale imaging of asphaltene-induced pore clogging in carbonate rocks. Fuel 283, 118871. https://doi.org/10.1016/J.FUEL.2020.118871.
- Liu, Q., Zhao, B., Santamarina, J.C., 2019. Particle migration and clogging in porous media: a convergent flow microfluidics study. J. Geophys. Res. Solid Earth 124, 9495–9504. https://doi.org/10.1029/2019JB017813.
- Marin, A., Lhuissier, H., Rossi, M., Kähler, C.J., 2018. Clogging in constricted suspension flows. Phys. Rev. E 97, 021102. https://doi.org/10.1103/PHYSREVE.97.021102/ FIGURES/5/MEDIUM.
- Markiewicz, A., Kiraga, M., Koda, E., 2022. Influence of physical clogging on filtration performance of soil-geotextile interaction. Geosynth. Int. 29, 356–368. https://doi. org/10.1680/jgein.21.00033.
- Mondal, S., Wu, C.H., Sharma, M.M., 2016. Coupled CFD-DEM simulation of hydrodynamic bridging at constrictions. Int. J. Multiphas. Flow 84, 245–263. https://doi.org/10.1016/J.IJMULTIPHASEFLOW.2016.05.001.

- Pang, L., Shen, S., Ma, C., Ma, T., Zhang, R., Tian, C., Zhao, L., Liu, W., Wang, J., 2015. Deformability and size-based cancer cell separation using an integrated microfluidic device. Analyst 140, 7335–7346. https://doi.org/10.1039/C5AN00799B.
- Prempeh, K.O.K., Chequer, L., Badalyan, A., Bedrikovetsky, P., 2020. Effects of the capillary-entrapped phase on fines migration in porous media. J. Nat. Gas Sci. Eng. 73, 103047 https://doi.org/10.1016/J.JNGSE.2019.103047.
- Saparbayeva, N., Balakin, B.V., 2023. CFD-DEM model of plugging in flow with cohesive particles. Sci. Rep. 131 (13), 1–9. https://doi.org/10.1038/s41598-023-44202-7, 2023
- Shin, H., Santamarina, J.C., 2010. Fluid-driven fractures in uncemented sediments: underlying particle-level processes. Earth Planet Sci. Lett. 299, 180–189. https://doi. org/10.1016/J.EPSL.2010.08.033.
- Song, Y., Ranjith, P.G., Wu, B., 2021. A study of ellipsoidal and spherical particle flow, clogging and unclogging dynamics. Powder Technol. 392, 424–437. https://doi.org/ 10.1016/J.POWTEC.2021.07.017
- Sun, H., Xu, S., Pan, X., Shi, L., Geng, X., Cai, Y., 2019. Investigating the jamming of particles in a three-dimensional fluid-driven flow via coupled CFD-DEM simulations. Int. J. Multiphas. Flow 114, 140-153. https://doi.org/10.1016/J. LJMULTIPHASEFLOW.2019.01.017.
- Tahmasebi, P., 2023. A state-of-the-art review of experimental and computational studies of granular materials: properties, advances, challenges, and future directions. Prog. Mater. Sci. 138, 101157 https://doi.org/10.1016/J.PMATSCI.2023.101157.
- Tahmasebi, P., 2019. An optimization-based approach for modeling of complex particles. Powder Technol. 356 https://doi.org/10.1016/j.powtec.2019.08.027.
- Tahmasebi, P., Kamrava, S., 2019. A pore-scale mathematical modeling of fluid-particle interactions: thermo-hydro-mechanical coupling. Int. J. Greenh. Gas Control 83, 245–255. https://doi.org/10.1016/j.ijggc.2018.12.014.
- Todisco, F., Vergni, L., Ceppitelli, R., 2023. Modelling the dynamics of seal formation and pore clogging in the soil and its effect on infiltration using membrane fouling models. J. Hydrol. 618, 129208 https://doi.org/10.1016/J.JHYDROL.2023.129208.
- Tomac, I., Gutierrez, M., 2014. Fluid lubrication effects on particle flow and transport in a channel. Int. J. Multiphas. Flow 65, 143–156. https://doi.org/10.1016/j. ijmultiphaseflow.2014.04.007.
- Valdes, J.R., Carlos Santamarina, J., 2007. Particle transport in a nonuniform flow field: retardation and clogging. Appl. Phys. Lett. 90, 244101 https://doi.org/10.1063/ 1.2748850/128440.
- Wen, C.Y., 1966. Mechanics of fluidization. Chem. Eng. Prog. Symp. Ser. 100–111. Wyss, H.M., Blair, D.L., Morris, J.F., Stone, H.A., Weitz, D.A., 2006. Mechanism for
- Wyss, H.M., Blair, D.L., Morris, J.F., Stone, H.A., Weitz, D.A., 2006. Mechanism for clogging of microchannels. Phys. Rev. E - Stat. Nonlinear Soft Matter Phys. 74, 061402 https://doi.org/10.1103/PHYSREVE.74.061402/FIGURES/4/MEDIUM.
- Xia, J., Tian, H., Dou, B., Xiao, P., Zheng, J., Lai, X., 2023. Experimental Review: particle clogging in porous sandstone geothermal reservoirs during tail water reinjection. J. Hydrol. 625, 130066 https://doi.org/10.1016/J.JHYDROL.2023.130066.
- Xu, S., Sun, H., Cai, Y., Geng, X., 2020. Studying the orifice jamming of a polydispersed particle system via coupled CFD–DEM simulations. Powder Technol. 368, 308–322. https://doi.org/10.1016/J.POWTEC.2020.01.003.
- Xu, W.J., Dong, X.Y., 2021. Simulation and verification of landslide tsunamis using a 3D SPH-DEM coupling method. Comput. Geotech. 129, 103803 https://doi.org/10.1016/j.compgeo.2020.103803.
- Ye, X., Cheng, Z., Wu, M., Hao, Y., Lu, G., Hu, B.X., Mo, C., Li, Q., Wu, Jianfeng, Wu, Jichun, 2022. Effects of clay minerals on the transport of polystyrene nanoplastic in groundwater. Water Res. 223, 118978 https://doi.org/10.1016/J.WATRES.2022.118978.
- Yin, Y., Cui, Y., Jing, L., 2024. Clogging and unclogging of fine particles in porous media: micromechanical insights from an analog pore system. Water Resour. Res. 60, e2023WR034628 https://doi.org/10.1029/2023WR034628.
- Zhang, W., Luo, J., Ding, L., Jaffrin, M.Y., 2015. A review on flux decline control strategies in pressure-driven membrane processes. Ind. Eng. Chem. Res. 54, 2843–2861. https://doi.org/10.1021/IE504848M/SUPPL_FILE/IE504848M_SI_001.
- Zhang, X., Tahmasebi, P., 2023. Drafting, kissing and tumbling process of two particles: the effect of morphology. Int. J. Multiphas. Flow 160, 104379. https://doi.org/ 10.1016/J.IJMULTIPHASEFLOW.2023.104379.
- Zhang, X., Tahmasebi, P., 2022. Coupling irregular particles and fluid: complex dynamics of granular flows. Comput. Geotech. 143, 104624 https://doi.org/10.1016/j. compgeo.2021.104624.
- Zhang, X., Tahmasebi, P., 2019. Effects of grain size on deformation in porous media. Transport Porous Media 129, 321–341. https://doi.org/10.1007/s11242-019-01291-1.
- Zhang, X., Tahmasebi, P., 2018. Micromechanical evaluation of rock and fluid interactions. Int. J. Greenh. Gas Control 76, 266–277. https://doi.org/10.1016/J. LJGGC.2018.07.018.
- Zhou, K., Hou, J., Sun, Q., Guo, L., Bing, S., Du, Q., Yao, C., 2018. A Study on Particle Suspension Flow and Permeability Impairment in Porous Media Using LBM–DEM–IMB Simulation Method. Transp, vol. 124. Porous Media, pp. 681–698. https://doi.org/10.1007/S11242-018-1089-Z/FIGURES/13.
- Zhou, Y., Zhou, B., Li, J., Wang, H., 2017. Study on the multi-sphere method modeling the 3D particle morphology in DEM. Springer Proc. Phys. 188, 601–608. https://doi. org/10.1007/978-981-10-1926-5_62/FIGURES/4.
- Zuriguel, I., Parisi, D.R., Hidalgo, R.C., Lozano, C., Janda, A., Gago, P.A., Peralta, J.P., Ferrer, L.M., Pugnaloni, L.A., Clément, E., Maza, D., Pagonabarraga, I., Garcimartín, A., 2014. Clogging transition of many-particle systems flowing through bottlenecks. Sci. Rep. 41 (4), 1–8. https://doi.org/10.1038/srep07324, 2014.